Reconstruction from Uncalibrated Affine Silhouettes

Paul McIlroy
http://mi.eng.cam.ac.uk/~pmm33
Tom Drummond
http://mi.eng.cam.ac.uk/~twd20

Machine Intelligence Laboratory
Department of Engineering
University of Cambridge
Cambridge, UK

Abstract

A method for recovering structure and motion from a set of scaled orthographic silhouette views with unconstrained camera motion is presented. The outer epipolar tangencies between six or more views are used simultaneously to recover the relative pose of the cameras and hence the visual hull of the object. The camera representation proposed permits a closed form solution in the optimization of the camera parameters. The resulting system is applied to the problem of reconstructing aircraft in flight.

1 Introduction

Structure and motion is a central problem in computer vision and approaches vary according to the problem setting. If features are available for matching, point correspondences place constraints on the spatial configuration of the scene and motion compatible with the camera views [13]. Smooth textureless objects do not readily provide features for matching and an alternative class of algorithms exists to tackle this problem using the outline in silhouette views [6].

In this paper we address the problem of model building in environments we do not control. An example problem is the reconstruction of aircraft geometry from images obtained from the ground. In this setting reliable feature matching is frustrated by a lack of contrast due to the high dynamic range in images taken against a bright sky background. The motion between the images is also unconstrained.

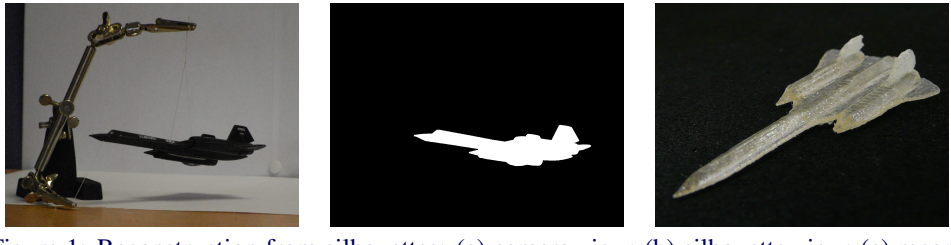

Figure 1: Reconstruction from silhouettes: (a) camera view; (b) silhouette view; (c) reconstructed model as output from a 3D printer in an acrylic-based photopolymer.

BMVC 2009 doi:10.5244/C.23.103

We show that using six or more unconstrained silhouette views it is possible to recover the geometry of the aircraft and the motion between the camera views using the two outer epipolar tangency constraints in each image.

1.1 Background

The maximum volume consistent with a set of silhouette views from a known camera configuration can be constructed as the intersection of the visual cones. This concept of the *visual hull* was introduced by Laurentini [14] based on volume intersection methods first proposed by Baumgart [3]. A general surface may contain concave regions that are not visible from any silhouette view, but the visual hull provides a close approximation to the true object geometry in the aircraft example as aircraft design avoids such concavities. The aim of this work is therefore to recover the visual hull consistent with an uncalibrated set of silhouette views.

Before the visual hull can be constructed, the camera configuration must first be determined from the silhouette views. The underlying geometry theory for silhouette views has been developed to tackle this problem. Cipolla and Blake [2] considered how the deformation of the *apparent contours* or silhouettes relates to the geometry of the surface around the corresponding *contour generators*, the locus of points on the object separating the visible and occluded regions. Giblin and Weiss [12] and Reiger [17] considered the special case of rotation about an axis under orthographic projection with singularities at fixed points on the apparent contours that do not deform. Porrill and Pollard [16] found that the intersection of two contour generators from two discrete camera viewpoints provided a pair of point correspondences. Cipolla *et al*. [2, 8] considered how these *frontier points* could be used to generate epipolar constraints to determine the camera motion.

Shape from silhouette under circular motion has received attention as a practical method for robust and accurate model building in a controlled setting [15, 24]. Additional arbitrary views can be registered with the initial circular set to obtain improved reconstructions [22, 23]. An initial circular set with a minimum of three views under circular motion is required. Methods using stereo-rigs [9] or configuration of mirrors [10] have also been proposed. Cheung *et al*. [5] proposed a 3D reconstruction algorithm combining shape from silhouette with stereo for a rigid object undergoing arbitrary rigid motion. Sinha *et al*. [19] proposed a method for camera calibration using dynamic silhouettes from moving objects viewed by a network of cameras. Only the outer frontier points are required in each image as the epipolar constraints from frontier points across a number of frames may be considered simultaneously due to the fixed camera configuration.

Bottino and Laurentini [4] introduced the problem of shape from silhouette from unknown viewpoints. The case of orthographic viewing directions parallel to the same plane is considered in detail, but orthographic projection with unrestricted viewing directions is left as an open problem.

Approaches to unconstrained motion using the deformation of apparent contours have been considered for a sequence of images from a moving camera. Vijayakumar *et al*. [21] considered video sequences under scaled orthographic projection and Åström and Kahl [1] considered the deformation of apparent contours for the full projective camera using snakes to track the apparent contours and using all available epipolar tangencies in each image.

Furukawa *et al*. [11] considered structure and motion from frontier points for an affine camera. The proposed method uses all available (typically a dozen or fewer, but at least two) frontier points to enable pair-wise recovery of the affine projection matrices. The images of

$n \geq 4$ frontier points are required in both views for a robust solution. If only the two outer frontier points are available then the proposed method resorts to using tangent information along the image contour. This is avoided in practice as the tangent orientation is noisy and it is not clear how to best combine both types of information.

In this paper we propose a method for structure and motion that requires only the two outer frontier points without resorting to noisy tangent information along the image contour. We consider the epipolar tangency constraints in all $N(N-1)$ camera pairs simultaneously and optimize a cost function based on residuals perpendicular to the tangent direction. In our example problem the aircraft silhouette generates only two outer frontier points reliably. We show that using six or more such views it is possible to recover the geometry of the aircraft and the camera motion.

We employ a Lie group representation for the camera parameters that permits a closed form solution for the derivatives required in the optimization (see Varadarajan [20] or Sattinger and Weaver [18] for a good introduction to Lie groups and their algebras).

2 Camera model

We use the following parameterization for the scaled orthographic camera model. $\mathbf{R}$ is a 3×3 rotation matrix, (u_0, v_0) is the principal point and s is a scale parameter.

The principal point in our camera model is the projection of the world origin in the camera image. It is a function of the arbitrary 3D point chosen as the world origin and is not related to the physical optical centre of the camera and lens hardware. The world origin must therefore lie along the optical axis of every camera. Hence, using a scaled orthographic camera model, we can consider all camera centres to be coincident at the world origin. The mapping between a point $\mathbf{X}$ in world coordinates and the same point $\mathbf{X}_c$ expressed in camera coordinates is given by

$$\mathbf{X}_c = \mathbf{R}_c\mathbf{X}. \tag{1}$$

The scaled orthographic projection of $\mathbf{X}_c$ may be expressed as

$$\begin{bmatrix} u \\ v \end{bmatrix} = \begin{bmatrix} s & 0 & 0 \\ 0 & s & 0 \end{bmatrix} \mathbf{X}_c + \begin{bmatrix} u_0 \\ v_0 \end{bmatrix}. \tag{2}$$

3 Epipolar tangents

A silhouette is formed by the projection of a visible object onto a binary image plane. The silhouette outline that bounds the silhouette is comprised of a subset of the set of apparent contours. The apparent contours are the projections of the contour generators which divide the visible part from the occluded part of the object surface. The contour generators are functions of both the surface geometry and viewpoint. Contour generators corresponding to two distinct viewpoints of the same surface are, in general, different space curves. These space curves intersect at frontier points.

As the contour generators are tangent to the rays from their respective camera centres it follows that a frontier point and two camera centres form an epipolar plane which is tangent to the surface at the frontier point. There are two epipolar tangent planes in the pencil of epipolar planes through the baseline that touch the object at a single point, Figure 2(a). The projection of each epipolar tangent plane is an epipolar tangent line in both images. The two

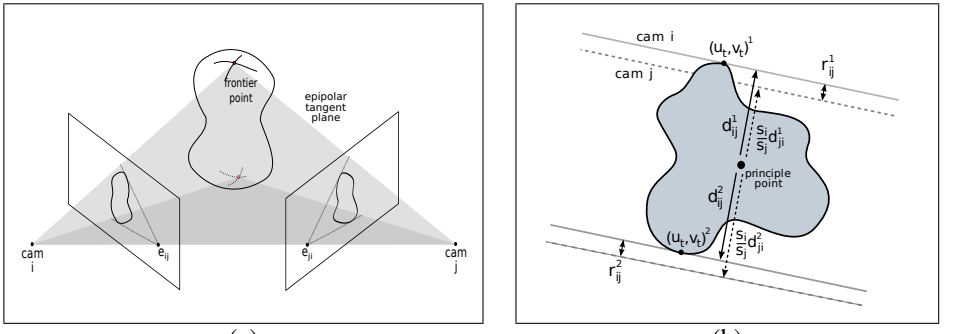

(a) (b)

Figure 2: Epipolar tangency constraints: (a) epipolar tangent planes for a perspective camera; (b) parallel epipolar lines and residual errors for an affine camera .

frontier points therefore project to the two points in each image where the epipolar lines touch the silhouette outline at a single point. These pairs of points may be used as correspondences to constrain the camera motion between the viewpoints.

In addition to the two outer frontier points, additional frontier points may be generated by certain configurations of surface geometry and viewpoints. Only the two outer frontier points are guaranteed to be present for all unoccluded objects. Considering only the outer two frontier points in the silhouette outlines reduces the problem of matching the pairs of points to one of two possible cases.

For the perspective camera model in Figure 2(a), the locations of the epipoles in both images are required to determine the epipolar tangent lines and corresponding tangent points. Using an affine camera model, the epipolar lines are parallel as shown in Figure 2(b). For the affine case, only the relative rotation between the cameras is required to determine the angle of the epipolar tangent lines and hence the corresponding epipolar tangent points in each image.

Each scaled orthographic camera has six parameters to be determined, three for the rotation relative to the world, two for the image coordinates of the principal point and one for the scale. Thus there are a total of $6N$ parameters in the N-camera system. The world reference frame may be chosen arbitrarily such that the first camera's rotation matrix is the identity, the principal point is in the centre of the image and it has unit scale. This constrains the world origin to lie on the optical axis of the first camera. By fixing one of the principal point coordinates in a second camera we fully specify the 3D position of the world origin. We have arbitrarily chosen seven of the $6N$ camera parameters in the system to define the world coordinate frame, leaving $(6N-7)$ free parameters to be solved using the constraints from the outer two epipolar tangents described in Section 3.

There are $\frac{1}{2}N(N-1)$ camera pairs in the system with each camera pair providing two unique constraints from the outer epipolar tangents, so for a unique solution the number of cameras, N, must satisfy

$$(6N-7) \geq N(N-1). \tag{3}$$

It is therefore possible to recover motion using the epipolar tangency constraint from a minimum of six silhouette views.

4 Epipolar constraints

The camera motion is obtained by an optimization process which minimises a cost function based on the epipolar tangents described in Section 3. The cost function is the sum of the squared residuals given by the perpendicular distance between the epipolar tangent point on the silhouette outline and the epipolar line corresponding to the epipolar tangent point in the second camera as illustrated in Figure 2(b). The cost function is expressed as

$$E = \sum_{i=1}^{N} \sum_{j=i+1}^{N} \sum_{k=1}^{2} (r_{ij}^{k})^2, \tag{4}$$

where r_{ij}^{k} is the residual error between the k^{th} epipolar tangent point in camera i and the epipolar line from camera j. The residual error may be expressed in terms of d_{ij}, the perpendicular distance from principal point to epipolar tangent line in camera i , and d_{ji}, the corresponding distance in camera j, such that

$$r_{ij} = d_{ij} - \frac{s_i}{s_j} d_{ji}, \tag{5}$$

where s_i and s_j are the scale parameters of cameras i and j respectively.

The direction in the i^{th} camera of an the epipolar tangent line from camera j is given by the X and Y components of

$$\begin{bmatrix} X \\ Y \\ Z \end{bmatrix} = \mathbf{R}_i \mathbf{R}_j^{-1} \begin{bmatrix} 0 \\ 0 \\ 1 \end{bmatrix}, \tag{6}$$

the z-axis of camera j projected into camera i. The length of the projected vector, $\left\| X \quad Y \right\|$, is equal to the magnitude of the sine of the angle between the two cameras' optical axes. This is given by the magnitude of the cross product between two unit vectors along the optical axes in world coordinates,

$$|\sin \rho_{ij}| = \left\| \mathbf{R}_i^{-1} \begin{bmatrix} 0 \\ 0 \\ 1 \end{bmatrix} \times \mathbf{R}_j^{-1} \begin{bmatrix} 0 \\ 0 \\ 1 \end{bmatrix} \right\|, \tag{7}$$

where ρ_{ij} is the angle between the two cameras' optical axes. We use this result to obtain a unit vector along the epipolar line,

$$\hat{e}_{ij} = \frac{1}{|\sin \rho_{ij}|} \begin{bmatrix} 1 & 0 & 0 \\ 0 & 1 & 0 \end{bmatrix} \mathbf{R}_i \mathbf{R}_j^{-1} \begin{bmatrix} 0 \\ 0 \\ 1 \end{bmatrix}. \tag{8}$$

The normal to the epipolar lines is given by

$$\hat{p}_{ij} = \begin{bmatrix} 0 & 1 \\ -1 & 0 \end{bmatrix} \hat{e}_{ij}, \tag{9}$$

thus the perpendicular distance between the epipolar tangent through silhouette point (u, v) and the principal point (u_0, v_0) is given by the dot product,

$$d_{ij} = \begin{bmatrix} u_i - u_{0i} \\ v_i - v_{0i} \end{bmatrix} \cdot \hat{p}_{ij}. \tag{10}$$

5 Optimization

The iterative optimization process begins with estimates for the camera parameters obtained by initialising the camera pose by hand. The cost function, eq. (4), is then minimized using the conjugate gradient method. The camera parameterization in Section 2 permits a closed form solution for the partial derivatives with respect to the camera parameters.

The partial derivatives with respect to the scale terms from eq. (5) are given by

$$\frac{\partial r_{ij}}{\partial s_i} = \frac{d_{ji}}{s_j}, \qquad \frac{\partial r_{ij}}{\partial s_j} = -\frac{d_{ji}}{s_j^2}. \tag{11}$$

From eq. (5) and (10) we obtain the partial derivatives with respect to the principal point,

$$\frac{\partial r_{ij}}{\partial u_{0_i}} = \begin{bmatrix} -1 \\ 0 \end{bmatrix} \cdot \hat{p}_{ij}, \qquad \frac{\partial r_{ij}}{\partial v_{0_i}} = \begin{bmatrix} 0 \\ -1 \end{bmatrix} \cdot \hat{p}_{ij}, \tag{12}$$

$$\frac{\partial r_{ij}}{\partial u_{0_j}} = -\frac{s_i}{s_j} \begin{bmatrix} -1 \\ 0 \end{bmatrix} \cdot \hat{p}_{ji}, \qquad \frac{\partial r_{ij}}{\partial v_{0_j}} = -\frac{s_i}{s_j} \begin{bmatrix} 0 \\ -1 \end{bmatrix} \cdot \hat{p}_{ji}. \tag{13}$$

Rotations form the Special Orthogonal Lie group, SO(3). We obtain the partial derivatives with respect to the camera rotations using the elements of the Lie algebra at the identity where,

$$\mathbf{R}^{t+1} = \mathfrak{M}\mathbf{R}^t. \tag{14}$$

$\mathfrak{M}$ describes the motion from $\mathbf{R}^t$ to $\mathbf{R}^{t+1}$ and is parameterized by $\mathbf{w}$, a vector in the Lie algebra, such that

$$\mathfrak{M} = \exp\{\mathbf{w}_\times\}, \tag{15}$$

$$\mathbf{w}_\times = \begin{bmatrix} 0 & -w_z & w_y \\ w_z & 0 & -w_x \\ -w_y & w_x & 0 \end{bmatrix}. \tag{16}$$

It follows that

$$\frac{\partial \mathfrak{M}}{\partial w_x} = \begin{bmatrix} 0 & 0 & 0 \\ 0 & 0 & -1 \\ 0 & 1 & 0 \end{bmatrix} = \mathbb{G}_0, \tag{17}$$

the generator for the first element of the Lie algebra. The partial derivative with respect to the x component of the motion of the i^{th} camera, $w_{x,i}$, is a function of the change in the epipolar line direction. From eq. (5) and (10),

$$\frac{\partial r_{ij}}{\partial w_{x,i}} = \begin{bmatrix} u_i - u_{0i} \\ v_i - v_{0i} \end{bmatrix} \cdot \frac{\partial \hat{p}_{ij}}{\partial w_{x,i}} + \frac{s_i}{s_j} \begin{bmatrix} u_j - u_{0i} \\ v_j - v_{0i} \end{bmatrix} \cdot \frac{\partial \hat{p}_{ji}}{\partial w_{x,i}}. \tag{18}$$

Combining eq. (9) with (8) gives,

$$\frac{\partial \hat{p}_{ij}}{\partial w_{x,i}} = \frac{\partial}{\partial w_{x,i}} \left\{ \frac{1}{|\sin \rho_{ij}|} \cdot \begin{bmatrix} 0 & -1 & 0 \\ 1 & 0 & 0 \end{bmatrix} \mathbf{R}_i \mathbf{R}_j^{-1} \begin{bmatrix} 0 \\ 0 \\ 1 \end{bmatrix} \right\}. \tag{19}$$

The camera rotation, $\mathbf{R}_i$, and the angle between the optical axes for the camera pair, ρ_{ij}, are functions of $w_{x,i}$. Applying the quotient rule,

$$\frac{\partial \hat{p}_{ij}}{\partial w_{x,i}} = \frac{1}{|\sin\rho_{ij}|}\begin{bmatrix}0 & -1 & 0\\ 1 & 0 & 0\end{bmatrix}\frac{\partial\{\mathbf{R}_i\}}{\partial w_{x,i}}\mathbf{R}_j^{-1}\begin{bmatrix}0\\0\\1\end{bmatrix} - \frac{\hat{p}_{ij}}{|\sin\rho_{ij}|}\frac{\partial\{|\sin\rho_{ij}|\}}{\partial w_{x,i}}, \tag{20}$$

where the partial derivative of the rotation matrix is given by the generator of the Lie algebra,

$$\frac{\partial\{\mathbf{R}_i\}}{\partial w_{x,i}} = \frac{\partial}{\partial w_{x,i}}\{\mathfrak{M}\mathbf{R}_i\} = \mathbb{G}_0\mathbf{R}_i. \tag{21}$$

Before considering the partial derivative of $|\sin\rho_{ji}|$ we first examine the second term in eq. (18) which is a function of the change in the perpendicular distance in the second camera of the pair as the first camera is rotated. The partial derivative of p_{ji}, the vector in the j^{th} camera perpendicular to the epipolar lines from camera i, is given by

$$\frac{\partial \hat{p}_{ji}}{\partial w_{x,i}} = \frac{1}{|\sin\rho_{ji}|}\begin{bmatrix}0 & -1 & 0\\ 1 & 0 & 0\end{bmatrix}\mathbf{R}_j\frac{\partial\{\mathbf{R}_i^{-1}\}}{\partial w_{x,i}}\begin{bmatrix}0\\0\\1\end{bmatrix} - \frac{\hat{p}_{ji}}{|\sin\rho_{ji}|}\frac{\partial\{|\sin\rho_{ji}|\}}{\partial w_{x,i}}. \tag{22}$$

requiring the partial derivative of the inverse of the rotation matrix,

$$\frac{\partial\{\mathbf{R}_i^{-1}\}}{\partial w_{x,i}} = \frac{\partial}{\partial w_{x,i}}\left\{(M\mathbf{R}_i)^{-1}\right\} = \mathbf{R}_i^{-1}(-\mathbb{G}_0). \tag{23}$$

The partial derivative of $|\sin\rho_{ij}|$ with respect to the camera motion is derived from eq. 7. Setting $\mathbf{s}$ as the cross product between the optical axes,

$$\frac{\partial|\sin\rho_{ij}|}{\partial w_{x,i}} = \|\mathbf{s}\| = (\mathbf{s}\cdot\mathbf{s})^{\frac{1}{2}} = \frac{1}{2}(\mathbf{s}\cdot\mathbf{s})^{-\frac{1}{2}}(2\mathbf{s}\frac{\partial\mathbf{s}}{\partial w_{x,i}}) = \frac{1}{|\sin\rho_{ij}|}\mathbf{s}\frac{\partial\mathbf{s}}{\partial w_{x,i}}, \tag{24}$$

hence substituting for $\mathbf{s}$ and applying the chain rule using eq. 23,

$$\frac{\partial\{|\sin\rho_{ij}|\}}{\partial w_{x,i}} = \frac{1}{|\sin\rho_{ij}|}\left(R_i^{-1}\begin{bmatrix}0\\0\\1\end{bmatrix}\times R_j^{-1}\begin{bmatrix}0\\0\\1\end{bmatrix}\right)\left(R_i^{-1}(-\mathbb{G}_0)\begin{bmatrix}0\\0\\1\end{bmatrix}\times R_j^{-1}\begin{bmatrix}0\\0\\1\end{bmatrix}\right). \tag{25}$$

The generators for the second and third elements of the Lie algebra yield the partial derivatives with respect to $w_{y,i}$ and $w_{z,i}$. The partial derivatives for p_{ij} and p_{ji} with respect to $w_{x,j}$, $w_{y,j}$ and $w_{z,j}$ are obtained by a similar method.

5.1 Smoothed tangent envelope

The epipolar tangent points corresponding to the updated epipolar lines must be determined at each iteration of the optimization. The mapping between the angle of the epipolar lines and the corresponding tangent points is a constant function of the silhouette in each view, so it makes sense to preprocess the silhouettes to extract the tangent envelope, depicted in Figure 3(a). In the method proposed by Sinha *et al.* [19] the convex hull of each silhouette is constructed, then an ordered list of the vertices is stored as a function of tangent angle.

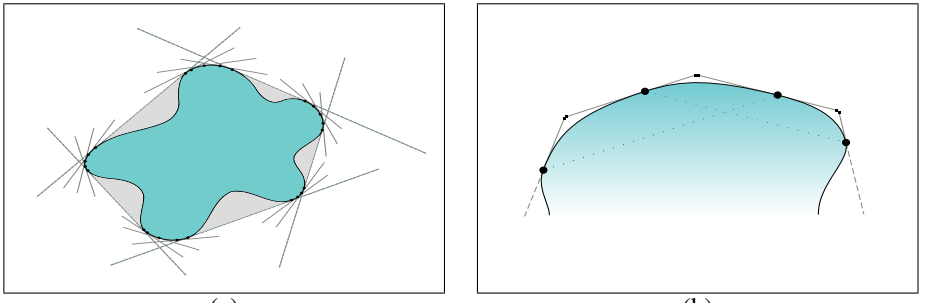

(a) (b)

Figure 3: Smoothed polygonal silhouettes: (a) tangent envelope; (b) smoothing.

The use of a continuous optimization method motivates the addition of a smoothing function to achieve a continuous mapping between tangent angle and tangent points. In our implementation the polygonal convex hull is smoothed by fitting Bézier curves between the vertices as illustrated in Figure 3(b). A distinction is made between convex regions of the silhouette boundary to be smoothed and concave regions. The tangent to the Bézier curve at each of the internal vertices along a convex section of the silhouette boundary is set as the angle from the previous vertex to the next. The tangent at each end of the convex boundary region is set as the angle between the last vertex in one convex region and the first vertex in the following one. The Bézier curve control points are set such that the increase in convex hull is small relative to the resolution of the segmentation process.

6 Experiments and results

We implemented the proposed system on an Intel Core 2 Duo E8500 3.16GHz with 4Gb RAM. Each iteration of the optimization takes 1.5ms, with a nine camera configuration typically taking 5-10 iterations to converge. Testing was conducted using data from three sources: synthetic data rendered from a 3D model with known ground truth, images of a model aircraft in a laboratory setting and images from internet video of an aircraft performing manoeuvres at an airshow.

The visual hull associated with each set of silhouettes is recovered by space carving using the camera configuration determined by the optimization. Figure 4(b) shows the reconstructed model of an SR-71 from high resolution images obtained in the laboratory and Figure 4(d) is the result for an F-22 using lower resolution images taken from the internet video. The SR-71 model was printed using a 3D printer to enable a physical comparison with the original object (Figure 1(c)).

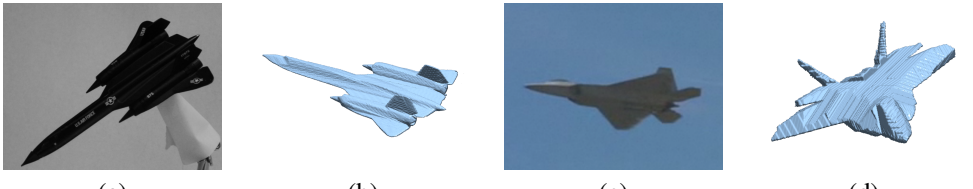

(a) (b) (c) (d)

Figure 4: Results: (a) SR-71 image (b) SR-71 model (c) F-22 video (d) F-22 model

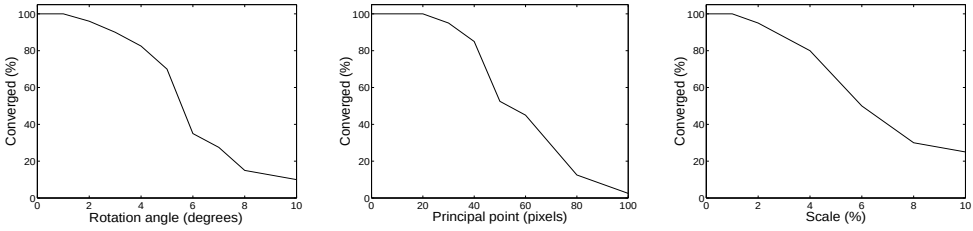

(a) (b) (c)

Figure 5: Radius of convergence of the initial camera configuration as a function of the Gaussian noise added to: (a) camera rotation; (b) principal point; (c) scale.

In an experiment designed to investigate the accuracy of the recovered camera configuration, the SR-71 was rotated through 90° with images captured at increments of 10°. The rotation angle between cameras was determined for the resulting camera configuration and the rms error for each interval was 0.27°. An error of this magnitude is expected in the manual positioning of the object. The rms error for the synthetic data was 0.02°.

The camera parameters must be initialised as a starting point for the optimization process. Figure 5 shows the radius of convergence with respect to camera parameters for a nine camera configuration with real data. The initial camera parameters supplied to the optimization process are randomly perturbed around the correct values by Gaussian noise with increasing variance. The system is considered to have converged to the correct result if all camera rotations are within 0.1° of the truth obtained at global minimum, the principal points are correct to 1.0 pixels and the scale parameters are correct to within 1.0%. In the example problem of reconstruction from images obtained at an airshow we find it is possible to set the initial camera pose to within 2° rotation by hand. Multiple attempts may be required to find the true configuration due to the presence of local minima. The optimization is robust to error in the initial estimate for the principal point. We also find that it is possible to initialise the scale by hand to sufficient accuracy for the aircraft example.

7 Discussion and future work

The success of optimization process is particularly sensitive to the camera rotation parameters in the initialisation as they determine the angle of the epipolar lines between camera pairs. If these are too far from the truth then the estimate for the tangent point may move beyond the local region and jump to an entirely separate region of the silhouette outline. Future work will consider an alternative to the simple non-linear optimization method that is more robust to the presence of local minima.

Six epipolar tangencies are required in each camera in order to constrain the six camera parameters. A single tangent point on the silhouette may provide up to two constraints if epipolar tangent lines from two cameras intersect at that point. If more than two epipolar tangent lines intersect at a single point then constraints are lost. This leads to a failure mode in objects with very high curvature in a configuration such that all epipolar lines intersect at two points on opposite extremes of the silhouette. In the aircraft example problem the views were chosen to avoid this configuration. By considering the backward propagation of covariance for the camera parameters it may be possible to automate the selection of a subset of views to ensure that the cameras are all well constrained.

8 Conclusion

We have presented a method for reconstructing an unknown object from six or more uncalibrated scaled-orthographic camera views using only the outer epipolar tangencies. A closed form solution for the partial derivatives of residual error with respect to camera parameters is obtained using a Lie group representation for the camera rotations. We applied the proposed method to the problem of reconstruction from images of an aircraft in flight as an example of model building in an uncontrolled environment.

Acknowledgements

The authors wish to thank Dr Gerhard Reitmayr and Dr Edward Rosten for their significant contribution to this work. This research is supported by the EPSRC.

References

[1] K. Åström and F. Kahl. Motion estimation in image sequences using the deformation of apparent contours. *IEEE Transactions on Pattern Analysis and Machine Intelligence*, 21(2):114–127, 1999.

[2] K. Åström, R. Cipolla, and P. Giblin. Generalised epipolar constraints. *International Journal of Computer Vision*, 33(1):51–72, 1999.

[3] B.G. Baumgart. *Geometric modeling for computer vision.* PhD thesis, 1974.

[4] A. Bottino and A. Laurentini. Introducing a new problem: Shape-from-silhouette when the relative positions of the viewpoints is unknown. *IEEE Transactions on Pattern Analysis and Machine Intelligence*, 25(11):1484–1493, 2003.

[5] G.K.M. Cheung, S. Baker, and T. Kanade. Visual hull alignment and refinement across time: A 3d reconstruction algorithm combining shape-from-silhouette with stereo. In *Proc. IEEE Computer Society Conference on Computer Vision and Pattern Recognition*, 2003.

[6] R. Cipolla. The visual motion of curves and surfaces. *Philosophical Transactions of the Royal Society A: Mathematical, Physical and Engineering Sciences*, 356(1740): 1103–1121, 1998.

[7] R. Cipolla and A. Blake. Surface shape from the deformation of apparent contours. *International Journal of Computer Vision*, 9(2):83–112, 1992.

[8] R. Cipolla, K.E. Åström, and P.J. Giblin. Motion from the frontier of curved surfaces. In *Proc. Fifth International Conference on Computer Vision*, 1995.

[9] K. Forbes, A. Voigt, and N. Bodika. Using silhouette consistency constraints to build 3D models. In *Proc. 14th Annual South African Workshop on Pattern Recognition*, 2003.

[10] K. Forbes, F. Nicolls, G. De Jager, and A. Voigt. Shape-from-silhouette with two mirrors and an uncalibrated camera. In *Proc. Ninth European Conference on Computer Vision*, 2006.

[11] Y. Furukawa, A. Sethi, J. Ponce, and D.J. Kriegman. Robust structure and motion from outlines of smooth curved surfaces. *IEEE Transactions on Pattern Analysis and Machine Intelligence*, 28(2):302–315, 2006.

[12] P. Giblin and R. Weiss. Reconstruction of surfaces from profiles. Technical report, University of Massachusetts, 1987.

[13] R. Hartley and A. Zisserman. *Multiple view geometry in computer vision*. Cambridge University Press, 2003.

[14] A. Laurentini. The visual hull concept for silhouette-based image understanding. *IEEE Transactions on Pattern Analysis and Machine Intelligence*, 16(2):150–162, 1994.

[15] P.R.S. Mendonça, K.Y.K. Wong, and R. Cippolla. Epipolar geometry from profiles under circular motion. *IEEE Transactions on Pattern Analysis and Machine Intelligence*, 23(6):604–616, 2001.

[16] J. Porrill and S. Pollard. Curve matching and stereo calibration. *Image and Vision Computing*, 9(1):45–50, 1991.

[17] J.H. Rieger. Three-dimensional motion from fixed points of a deforming profile curve. *Optics Letters*, 11(3):123–125, 1986.

[18] D.H. Sattinger and O.L. Weaver. *Lie groups and algebras with applications to physics, geometry, and mechanics*. Springer-Verlag New York, 1986.

[19] S.N. Sinha, M. Pollefeys, and L. McMillan. Camera network calibration from dynamic silhouettes. In *Proc. IEEE Computer Society Conference on Computer Vision and Pattern Recognition*, 2004.

[20] V.S. Varadarajan. *Lie groups, Lie algebras, and their representations*. Prentice-Hall, 1974.

[21] B. Vijayakumar, D.J. Kriegman, and J. Ponce. Structure and motion of curved 3D objects from monocularsilhouettes. In *Proc. IEEE Computer Society Conference on Computer Vision and Pattern Recognition*, 1996.

[22] K.Y.K. Wong and R. Cipolla. Structure and motion from silhouettes. In *Proc. Eighth IEEE International Conference on Computer Vision*, 2001.

[23] K.Y.K. Wong and R. Cipolla. Reconstruction of sculpture from its profiles with unknown camera positions. *IEEE Transactions on Image Processing*, 13(3):381–389, 2004.

[24] K.Y.K. Wong, P.R.S. Mendonça, and R. Cipolla. Camera calibration from surfaces of revolution. *IEEE Transactions on Pattern Analysis and Machine Intelligence*, 25(2): 147–161, 2003.